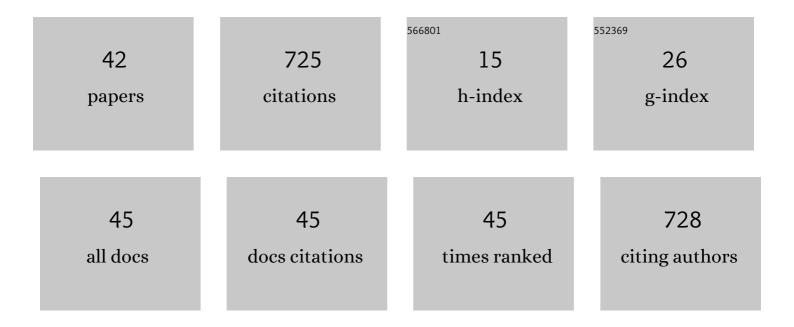
George A Kastis

List of Publications by Year in descending order

Source: https://exaly.com/author-pdf/3009498/publications.pdf

Version: 2024-02-01



#	Article	IF	CITATIONS
1	Discrete Shearlets as a Sparsifying Transform in Low-Rank Plus Sparse Decomposition for Undersampled (k, t)-Space MR Data. Journal of Imaging, 2022, 8, 29.	1.7	2
2	Evaluation of the Spline Reconstruction Technique for Preclinical PET Imaging. Computer Methods and Programs in Biomedicine, 2022, 217, 106668.	2.6	1
3	A few-shot U-Net deep learning model for lung cancer lesion segmentation via PET/CT imaging. Biomedical Physics and Engineering Express, 2022, 8, 025019.	0.6	20
4	Reconstruction of Preclinical PET Images via Chebyshev Polynomial Approximation of the Sinogram. Applied Sciences (Switzerland), 2022, 12, 3335.	1.3	3
5	Simple Formulae, Deep Learning and Elaborate Modelling for the COVID-19 Pandemic. Encyclopedia, 2022, 2, 679-689.	2.4	1
6	Covid-19: predictive mathematical formulae for the number of deaths during lockdown and possible scenarios for the post-lockdown period. Proceedings of the Royal Society A: Mathematical, Physical and Engineering Sciences, 2021, 477, 20200745.	1.0	7
7	SARS-CoV-2: The Second Wave in Europe. Journal of Medical Internet Research, 2021, 23, e22431.	2.1	10
8	Quantification of T1, T2 relaxation times from Magnetic Resonance Fingerprinting radially undersampled data using analytical transformations. Magnetic Resonance Imaging, 2021, 80, 81-89.	1.0	2
9	Mathematical models and deep learning for predicting the number of individuals reported to be infected with SARS-CoV-2. Journal of the Royal Society Interface, 2020, 17, 20200494.	1.5	53
10	A Spline Approach to Parallel-Hole Collimator Deblurring for aSRT-Reconstructed SPECT Images. , 2019, , .		0
11	A New Approach for the Inversion of the Attenuated Radon Transform. Springer Optimization and Its Applications, 2019, , 433-457.	0.6	1
12	The attenuated spline reconstruction technique for single photon emission computed tomography. Journal of the Royal Society Interface, 2018, 15, 20180509.	1.5	12
13	A Novel Metal-Based Imaging Probe for Targeted Dual-Modality SPECT/MR Imaging of Angiogenesis. Frontiers in Chemistry, 2018, 6, 224.	1.8	32
14	Automatic cumulative sums contour detection of FBP-reconstructed multi-object nuclear medicine images. Computers in Biology and Medicine, 2017, 85, 43-52.	3.9	3
15	Investigation of Image Reconstruction Parameters of the Mediso nanoScan PC Small-Animal PET/CT Scanner for Two Different Positron Emitters Under NEMA NU 4-2008 Standards. Molecular Imaging and Biology, 2017, 19, 550-559.	1.3	10
16	Radiolabeled methotrexate as a diagnostic agent of inflammatory target sites: A proof-of-concept study. Molecular Medicine Reports, 2017, 17, 2442-2448.	1.1	5
17	Cumulative sums for edge determination of a single object in PET and SPECT images. Journal of Physics: Conference Series, 2016, 738, 012010.	0.3	0

aSRT: A new analytic reconstruction algorithm for SPECT. , 2016, , .

GEORGE A KASTIS

#	Article	IF	CITATIONS
19	The SRT reconstruction algorithm for semiquantification in PET imaging. Medical Physics, 2015, 42, 5970-5982.	1.6	5
20	Mathematical Methods in PET and SPECT Imaging. , 2015, , 903-936.		3
21	Evaluation of the spline reconstruction technique for PET. Medical Physics, 2014, 41, 042501.	1.6	15
22	Boundary value problems and medical imaging. Journal of Physics: Conference Series, 2014, 490, 012017.	0.3	0
23	An analytic reconstruction method for PET based on cubic splines. Journal of Physics: Conference Series, 2014, 490, 012128.	0.3	1
24	Dose- and time-dependent effects of lipopolysaccharide on technetium-99-m-labeled diethylene-triamine pentaacetatic acid clearance, respiratory system mechanics and pulmonary inflammation. Experimental Biology and Medicine, 2013, 238, 209-222.	1.1	4
25	Evaluation of a Spline Reconstruction Technique for SPECT: Comparison with FBP and OSEM. , 2011, , .		4
26	Evaluation of a spline reconstruction technique: Comparison with FBP, MLEM and OSEM. , 2010, , .		8
27	Inspiratory Resistive Breathing Induces Acute Lung Injury. American Journal of Respiratory and Critical Care Medicine, 2010, 182, 1129-1136.	2.5	59
28	Analytical reconstructions for PET and spect employing L ¹ -denoising. , 2009, , .		1
29	Imaging recognition of inhibition of multidrug resistance in human breast cancer xenografts using 99mTc-labeled sestamibi and tetrofosmin. Nuclear Medicine and Biology, 2005, 32, 573-583.	0.3	19
30	Compact CT/SPECT Small-Animal Imaging System. IEEE Transactions on Nuclear Science, 2004, 51, 63-67.	1.2	77
31	Imaging recognition of multidrug resistance in human breast tumors using 99mTc-labeled monocationic agents and a high-resolution stationary SPECT system. Nuclear Medicine and Biology, 2004, 31, 53-65.	0.3	24
32	99mTc glucarate high-resolution imaging of drug sensitive and drug resistant human breast cancer xenografts in SCID mice. Nuclear Medicine Communications, 2004, 25, 711-720.	0.5	16
33	High-resolution imaging with (99m)Tc-glucarate for assessing myocardial injury in rat heart models exposed to different durations of ischemia with reperfusion. Journal of Nuclear Medicine, 2004, 45, 1251-9.	2.8	20
34	Evaluating estimation techniques in medical imaging without a gold standard: experimental validation. , 2003, 5034, 230.		7
35	Tomographic small-animal imaging using a high-resolution semiconductor camera. IEEE Transactions on Nuclear Science, 2002, 49, 172-175.	1.2	44
36	Objective comparison of quantitative imaging modalities without the use of a gold standard. IEEE Transactions on Medical Imaging, 2002, 21, 441-449.	5.4	43

GEORGE A KASTIS

#	Article	IF	CITATIONS
37	Estimation in Medical Imaging without a Gold Standard. Academic Radiology, 2002, 9, 290-297.	1.3	49
38	Quantitative analysis of acute myocardial infarct in rat hearts with ischemia-reperfusion using a high-resolution stationary SPECT system. Journal of Nuclear Medicine, 2002, 43, 933-9.	2.8	84
39	Objective Comparison of Quantitative Imaging Modalities Without the Use of a Gold Standard. Lecture Notes in Computer Science, 2001, , 12-23.	1.0	3
40	Gamma-ray imaging using a CdZnTe pixel array and a high-resolution, parallel-hole collimator. IEEE Transactions on Nuclear Science, 2000, 47, 1923-1927.	1.2	39
41	Shock wave and cavitation bubble dynamics during photodisruption in ocular media and their dependence on the pulse duration. , 1996, , .		11
42	Time-resolved observations of shock waves and cavitation bubbles generated by femtosecond laser pulses in corneal tissue and water. , 1996, 19, 23.		9